A COMPARATIVE STUDY OF THREE METHODOLOGIES FOR MODELING DYNAMIC STALL

L. N. Sankar
School of Aerospace Engineering
Georgia Tech, Atlanta, GA 30332-0150

J. Zibi-Bailly, J. C. LeBalleur, D. Blaise
Office National d'Etudes et de Recherches Aérospatiales
Châtillon – 92322 - France

O. Rouzaud
Office National d'Etudes et de Recherches Aérospatiales
Toulouse – 31055 – France

M. Rhee
Army / NASA Rotorcraft Division
Aeroflightdynamics Directorate (AMRDEC)
US Army Aviation and Missile Command
Ames Research Center, Moffett Field, CA 94035-1099

ABSTRACT

Numerical simulations are presented for a NACA0015 airfoil undergoing sinusoidal pitching motion. Three different approaches are presented: Navier-Stokes simulations with an alternating direction implicit time marching scheme, Navier-Stokes simulations with an iterative time marching scheme, and a strongly coupled viscous-inviscid interaction approach. Results are presented for three cases: steady case, attached flow, and moderate stall. Among these cases, the moderate stall case is further analyzed to assess the effects of grid density, numerical viscosity and transition on the computed results.

It is found that all three methods give satisfactory results for the attached flow case. It is observed from the moderate stall case study that the transition point prediction plays a critical role in the prediction of airloads. The one - equation Spalart-Allmaras turbulence model used for moderate stall cases did not adequately predict the airloads, particularly the drag and pitching moment hysteresis. Finally, it is found that the combination of a coarse grid and high values of numerical viscosity can lead to thicker boundary layers and earlier separation, and can dramatically affect the computations.

INTRODUCTION

During the past two decades, there has been an increased reliance on the use of computational fluid dynamics methods for modeling rotors in high speed forward flight. Computational methods are being developed for modeling the shock induced loads on the advancing side, first-principles based modeling of the trailing wake evolution, and for retreating blade stall. The retreating blade dynamic stall problem has received particular attention, because the large variations in lift and pitching moments encountered in dynamic stall can lead to blade vibrations and pitch link fatigue. Ekaterinaris and Platzer present a comprehensive review of computational methods aimed at modeling dynamic stall [1].

It is necessary to carefully validate the CFD methods before these methods can be applied with confidence to rotor and airfoil design. Fortunately there are several excellent databases available for this purpose. During the 1970s, a research group headed by McCroskey, McAlister and Carr [2] developed a comprehensive set of hysteresis load data for several airfoils for a range of flow conditions. Other researchers (e.g., Carta at the United Technologies Research Center) have also experimentally studied dynamic stall phenomena [3-4]. There have been flow visualization studies by Werlé at ONERA [5], and by Carr and Chandrasekhara [6] that have shed light on the complex physics behind dynamic stall. The most recent of these databases is a comprehensive study done by Piziali for an oscillating NACA 0015 airfoil/wing [7]. In this work the effects of mean angle of attack, amplitude of oscillations, reduced frequency, transition point excursion, and tip relief effects on the measured loads have been systematically documented.

Under a US- France Memorandum of Agreement (MOA) in Helicopter Aeromechanics, the present researchers have been validating numerical methods for modeling dynamic stall phenomena. A coordinated effort is in place for validating these methods using Piziali's 2-D data base. This work presents the findings of this joint research.

MATHEMATICAL AND NUMERICAL FORMULATION

This paper is a comparative study of three different methods for modeling dynamic stall phenomena. The mathematical and numerical details behind these methods have been extensively published in open literature [8-22].

Therefore, in this work, only a brief description of the three approaches is given.

Georgia Tech RANS Implicit Time Marching method

In this approach, the Navier-Stokes (N-S) equations are solved in a body-fitted coordinate system. These equations may be formally written as:

$$\frac{\partial \hat{q}}{\partial \tau}+\frac{\partial \hat{E}}{\partial \xi}+\frac{\partial \hat{F}}{\partial \zeta}=\frac{\partial \hat{R}}{\partial \xi}+\frac{\partial \hat{S}}{\partial \zeta} \tag{1}$$

Here:

$$\hat{q}=\frac{1}{J}\begin{Bmatrix}\rho\\ \rho u\\ \rho v\\ \rho E\end{Bmatrix}$$

$$\hat{E}=\frac{1}{J}\begin{Bmatrix}\rho U\\ \rho u U+\xi_x p\\ \rho v U+\xi_y p\\ \rho U h_0-\xi_t p\end{Bmatrix} \quad \hat{F}=\frac{1}{J}\begin{Bmatrix}\rho V\\ \rho u V+\zeta_x p\\ \rho u V+\zeta_y p\\ \rho V h_0-\zeta_t p\end{Bmatrix}$$

$$\hat{R}=\frac{1}{J}\begin{Bmatrix}0\\ \xi_x\tau_{xx}+\xi_y\tau_{xy}\\ \xi_x\tau_{xy}+\xi_y\tau_{yy}\\ \xi_x(u\tau_{xx}+v\tau_{xy}+kT_x)+\xi_y(u\tau_{xy}+v\tau_{yy}+kT_y)\end{Bmatrix}$$

$$\hat{S}=\frac{1}{J}\begin{Bmatrix}0\\ \zeta_x\tau_{xx}+\zeta_y\tau_{xy}\\ \zeta_x\tau_{xy}+\zeta_y\tau_{yy}\\ \zeta_x(u\tau_{xx}+v\tau_{xy}+kT_x)+\zeta_y(u\tau_{xy}+v\tau_{yy}+kT_y)\end{Bmatrix}$$

Here ρ is density; u, v are the Cartesian components of fluid velocity; T is the temperature; and p is the pressure. The quantities τ_{xx}, τ_{xy}, and τ_{yy} are the viscous stresses that are computed using Stokes' relations, with the molecular viscosity augmented by the eddy viscosity. The quantity k is the thermal conductivity of the fluid, augmented by eddy conductivity. The quantity J is the Jacobian of transformation, while (ξ_x, ξ_y, ζ_x, ζ_y) are the metrics of transformation. U and V are called the contravariant components of velocity, and may be written as:

$$\begin{aligned}U&=(u-x_\tau)\xi_x+(v-y_\tau)\xi_y\\ V&=(u-x_\tau)\zeta_x+(v-y_\tau)\zeta_y\end{aligned} \tag{2}$$

Here x_τ and y_τ are the velocities of the points on the grid in an inertial frame, associated with the pitching motion of the airfoil. These quantities can be analytically computed if the airfoil motion is specified.

Standard second order accurate central differences are used to approximate the spatial derivatives and the metrics in the above equations. The temporal derivative is approximated by a two point backward difference formula. This discretization leads to a system of nonlinear simultaneous equations for the flow properties at each time step, which may be formally written as follows:

$$\frac{\hat{q}^{n+1}-\hat{q}^n}{\Delta t}=\frac{\Delta q^{n+1}}{\Delta t}=R^{n+1} \tag{3}$$

Here 'n' refers to the time level where the solution is known, and 'n+1' is the next time step. The time step is given by Δt.

Use of central differences to approximate the derivatives in equation (1) can lead to an odd-even decoupling of the solution, which exhibit themselves as oscillations in the solution of wavelength 2 Δξ and 2 Δη. These oscillations are filtered out using the well known Jameson-Turkel-Schmidt filter made of blended second and fourth differences of the flow properties [21]. The filter terms are multiplied by a factor that varies from 0.2 to 0.5. This is the same order as the coefficient found in the numerical viscosity term in approximate Riemann solvers [22].

The above equations are solved by linearizing the right hand side of equation (3) about the previous time level so that to the following form results:

$$\left[I-\Delta t\frac{\partial R}{\partial \hat{q}}\right]\Delta\hat{q}^{n+1}=\Delta t R^n \tag{4}$$

The above may be viewed as a sparse penta-diagonal system of simultaneous equations. The matrix is approximately factored into two tri-diagonal matrices as discussed by Beam and Warming [23]. The tridiagonal matrices are easily inverted using the Thomas algorithm. Once $\Delta\hat{q}^{n+1}$ is known, the flow properties may be updated as

$$\hat{q}^{n+1}=\hat{q}^n+\Delta q^{n+1} \tag{5}$$

Full linearization of the Jameson-Turkel-Schmidt filter term would increase the bandwidth of the matrix on the left hand side, requiring block-penta-diagonal inversion of the matrices. Therefore, a simple second difference filter is used on the left hand side. For additional details of the Georgia Tech method, the reader is referred to Ref. 8.

ONERA Navier-Stokes method

The ONERA Navier-Stokes code [9] is a multidomain solver for structured grids with a cell-centered finite-volume discretization. The numerical scheme corresponds to the Jameson's scheme [21], and uses the method of lines to decouple the spatial and temporal discretizations. The starting point in this approach is the same as equation (3), written in the following semi-discrete form:

$$\frac{\partial q}{\partial t}=R(q) \tag{6}$$

where R(q) represents the "residual" made of convective and diffusive fluxes. Second-order central differences are used for all spatial derivatives. As in the Georgia Tech solver, the residual R(q) includes a blend of linear 4^{th}-difference-based and 2^{nd}-difference-based artificial dissipation term. This

dissipation term is needed to suppress the odd-even decoupling and to prevent the appearance of oscillations in the neighborhood of shock waves or stagnation points.

When only the steady state solution is of interest, a variety of convergence acceleration techniques are available including local time stepping, FAS multigrid method [10] using V-cycles, and the implicit residual smoothing of Lerat *et al.* [11].

In unsteady flow applications, although a global time stepping algorithm is implemented [12], we have used the dual-time stepping method [13,14,24], which is very efficient for simulating low-frequency phenomena. It consists in the resolution of the unsteady equations with a time-marching steady-state solver using the usual acceleration techniques, while providing a second-order time accuracy. The governing equations are reformulated with the introduction of a dual time step τ, such as :

$$\frac{\partial q}{\partial \tau} + \frac{\partial q}{\partial t} + R(q) = \frac{\partial q}{\partial \tau} + R^*(q) = 0 \qquad (7)$$

where R(q) is the residual term which contains the convective, diffusive and artificial dissipation fluxes, R*(q) is the unsteady residual. Sub-iterations are done until R*(q) reaches a tolerence criterium. When the iterations converge at every time step, the discretized form of the unsteady Navier-Stokes equations is satisfied.

For turbulent computations, several turbulence models are available, including Baldwin-Lomax, Spalart-Allmaras, k-ε of Launder Sharma, and k-l model of Smith.

The present computations require the following boundary conditions. At the wall, the relative viscosity is zero because of the no-slip condition. At the airfoil surface adiabatic conditions are applied. Non-reflecting conditions are applied at the far field boundaries. At the wake cut, continuity of the conservative variables is ensured.

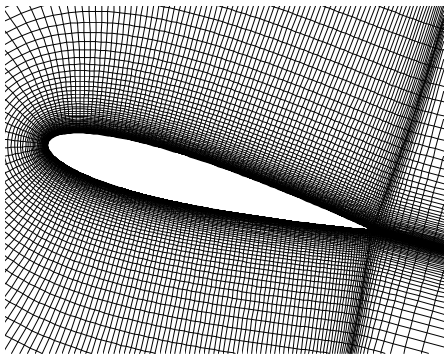


Figure 1- Common grid (257x129) for RANS solvers.

Grid Generations for N.S. Calculations: The C-grid around the airfoil was constructed with a hyperbolic grid generator developed at ONERA. This grid generator ensures the regularity and the orthogonality of the mesh, which are very important for adequately resolving the boundary layer.

A medium grid has been generated for the GIT and ONERA Navier-Stokes calculations with 257 points in the chordwise direction and 129 points in the normal direction to the airfoil. The outer boundary of the grid is located approximately 20 chords away from the airfoil. The first point off the solid wall is placed so that the value of y^+ is less than 1 near the leading edge.

Turbulence Models for N.S. calculations: The one equation transport model of Spalart-Allmaras [27] is used in the present computations. A zero-equation Baldwin-Lomax equation model has also been used when the flow is attached. These models are employed "as is" without any changes or adjustments to the constants in the models. In both the Georgia Tech and ONERA Navier-Stokes analyses, the RANS and turbulent equations systems are decoupled from each other, so that the eddy viscosity lags the mean flow properties by one time step.

The Spalart-Allmaras model is integrated in time in the Georgia Tech analysis using an implicit time marching algorithm that is identical in form to the mean flow algorithm. The convection terms are approximated by two-point upwind schemes. In the ONERA RANS method, the turbulent equations are discretized on the fine grid and solved with a multigrid strategy.

ONERA Viscous-Inviscid Interaction method

Formulation and scope : The generalized *viscous-inviscid interaction* (**VII**) considers that the "VII splitting-coupling" is a numerical technique (with two grids, two schemes) for simulating truncated or full RANS equations, and no more a zonal Prandtl approach. The VIS05 code, early developed and still extended by LeBalleur [16,17,18], is used in its time-consistent version [19].

The VII splitting follows LeBalleur's "Defect-Formulation theory" [16,21,17,18] for the full RANS Navier-Stokes equations. A thin-layer approximation, where however a non-zero normal pressure gradient is maintained by the theory, was used in the present work. This thin layer approximation enables lower cost solutions, that are still valid at deep stall, due to the "Displacement-Referential" and viscous-inviscid overlay of the theory [18,17,16,21,22].

An advantage of the VIS05 code, that splits the solution with two distinct viscous / inviscid schemes and solves them on two distinct adaptive overlaying grids, is to have a very low numerical diffusion. This makes it sure to obtain for example, contrary to RANS solvers, in the whole viscous path upstream separation, an effective numerical capture by the grid of the proper boundary layer thickness that results from the turbulent models, and not only $y^+=1$ fulfillment. This is a crucial key in stall prediction.

Numerical components of VIS05 : *The viscous layer* is solved by a hybrid "field-integral" technique, specific to VIS codes, with z-discretised velocity and density profiles. The profiles are parametrically modeled, and are designed for attached or deeply separated flows as discussed in

Ref.[16,17,18,21]. At each station, the flow profiles are discretised in the direction normal to the local interacting inviscid streamlines. This viscous discretisation, as formulated by LeBalleur [16, 17], is non-linearly implicit in time and space, marching in space, second-order in space (or first-order in areas of coarse grid), grid-adaptive to the thickness and gradient of the velocity profiles, with an automated switch between the "direct" mode of solution (pressure prescribed), and an "inverse" mode (inviscid normal-velocity at wall or wake-cut prescribed).

The VII coupling is time-consistently strong. It is converged at each time-step, using the "Massive-separation" [17,18] level of LeBalleur's "Semi-inverse" algorithm [20,21]. It includes a stability control, that computes at each wall / wake node the stabilizing local relaxation coefficients, for both the direct and the inverse modes of calculation of the viscous solution. This control is capable of yielding stabile solutions on clustered grids, even when massive separation and deep stall is present.

The inviscid field (in the version used) is solved using the full unsteady potential equation. An implicit time marching scheme is used, with an iterative SLOR technique at each time-step. These iterations on the inviscid flow are combined with the viscous-inviscid iterations that yield the time-consistently strong VII coupling, and the full viscous upstream influence recovery. A second-order centered discretisation in space [17,18], and LeBalleur's rotated upwind discretisation of spatio-temporal terms at subsonic speeds [19], are used, with a first-order option in time.

Self-adaptive VIS05 grid : The VIS05 code uses a self-adaptation of the viscous and inviscid C-grids (i-k) for automatically capturing the wake geometry, and includes additional self-adaptation of the VIS05 grid to the capture of viscous phenomena, LeBalleur [18,17,16]. Each time-step (Figure 2), in the k-direction normal to the viscous layer, the discretisation is self-adapted at all i-stations, both to the boundary-layer edge, distributing 49 nodes between wall or wake-center and the outer boundary layer edge δ, and to the maximal normal velocity gradient, concentrating the 49 nodes in the outer mixing-layer where deep separation occur.

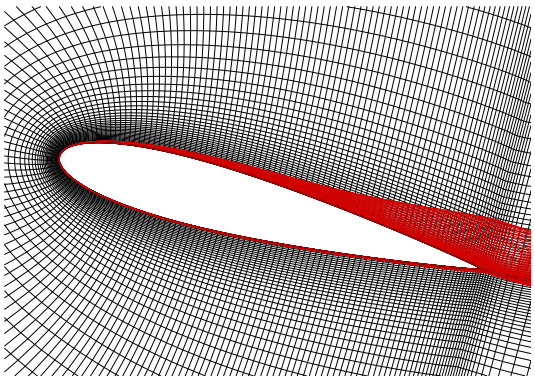


Figure 2 – Instantaneous VIS05 viscous-inviscid grid (moderate stall, k=0.038, α=15^o upstroke, 257x(64+49)).

Turbulence VIS05 model: The code uses the LeBalleur two-equation k-$\overline{u'v'}$ model [16,21,17,18], denoted "k-u'v' forced by parametric profiles". The forcing profiles here deal not only with the mean-flow, but also with the quantities of turbulence, so making the model robust in separated flow, and free of an excessive weight of the wall regions.

Transition-intermittency VIS05 model: The beginning of laminar-turbulent transition is either prescribed, or modeled at each time-step by VIS05, based on a trend toward laminar separation, or on a quasi-steady Michel's criterion.

An intermittency model is also used in the transitional zones, contrary to the RANS methods. In the temporary present status and modality of use, if a laminar separation triggers transition, the intermittency model forces the transition to occur and to be completed somewhat upstream laminar separation. This temporary mode delays any transitional leading-edge bubble and transforms the laminar separation into a turbulent separation at a downstream location, which explains an insufficient decrease in the velocity suction peaks at leading-edge when transitional bubbles occur.

DESCRIPTION OF THE BENCHMARK EXPERIMENT MODELED IN THIS STUDY

The present comparative study makes extensive use of results from an experiment conducted by Piziali at US Army Aeroflightdynamics Directorate Ames Research center [7]. In this study, a rectangular semi-span wing made of NACA 0015 airfoil sections, as well as a 2-D configuration that spans from wall to wall, were tested. The model had a span of 60 inches, and a chord of 12 inches. The wing was untwisted. Experiments were done with and without boundary layer trips. However, the uncertainties arising from transition modeling cannot be removed. The height of the trips (compared to the computed incoming boundary layer) is expected both to trigger transition and to thicken the boundary layer with an (unmeasured) unknown amount. In the present study, the tripped experimental data are used in steady and unsteady attached flows, free transition ones at moderate stall.

The wing was instrumented with 100 pressure transducers located at nine spanwise locations for the complete 3-D wing case. For 2-D configuration, a total of 50 pressure transducers were used at four locations. Twenty additional absolute pressure transducers were installed at the mid - span location of this configuration. The present work makes extensive use of the pressure distribution at this location for code validation. The lift, drag, and pitching moment loads were computed through a numerical integration of the measured pressures. The measured pressure data was enriched using a specially developed interpolation to arrive at pressure data at a number of upper and lower surface stations, before load integration.

Both quasi-steady and the pitch oscillation test data were acquired. The quasi-steady data may be viewed as oscillating wing data at a very low physical frequency and was mostly a single cycle data. The pitch oscillation test data were collected for 20 cycles, and were ensemble - averaged to eliminate cycle to cycle variations. Instantaneous cycle-averaged pressure data is available at 256 closely spaced angles of attack during the cycle.

Reference 7 gives additional details of the experiment, and an extensive set of results for a number of 2-D and 3-D configurations, flow conditions, and oscillation frequencies.

RESULTS AND DISCUSSION

Calculations are presented for several different conditions in this work. In all the cases, the freestream Mach number was nominally 0.29, and the Reynolds number was nominally 1.95 million. In the Georgia Tech and ONERA RANS calculations, the flow was assumed to be fully turbulent. The ONERA VII used a transition model, and an intermittency model as discussed earlier.

Static Calculations

Figures 3-5 show the comparison of computed loads and experiment data. The experimental data presented here is quasi-steady data from a single cycle of oscillation at a very low reduced frequency, and had some hysteresis from the upstroke and downstroke motion. The computations were done at fixed angles of attack, one angle at a time, and are free of this hysteresis effect.

The above calculations indicate that the Georgia Tech methodology has a slightly smaller lift-curve slope than the other two methods, but stalls at approximately the same angle of attack as the experiment. The two ONERA methods predict the static stall to occur at 1 to 2 degrees later than the experiment. All the three methods predict the initial rise in the nose-up pitching moment with experiment well, but differ from each other in the prediction of moment stall. The ONERA Navier-Stokes method predicted moment stall to occur around 17 degrees, while the Georgia tech method, and the ONERA viscous-inviscid method, predict fairly well the occurrence of the moment stall around 14 degrees as in the experiment.

To understand the discrepancies between these three methods, the flow field was examined. Figure 6 shows the streamline plots at a typical angle of attack (14 degrees). It is seen that the extent of the separated flow region, as predicted by the Georgia Tech N-S methodology is somewhat larger than that predicted by the two ONERA methodologies. The larger separation region found in the Georgia Tech simulation can be related to the previous loads evolutions. Some speculations on the reasons for these discrepancies are given later as part of a moderate stall simulation.

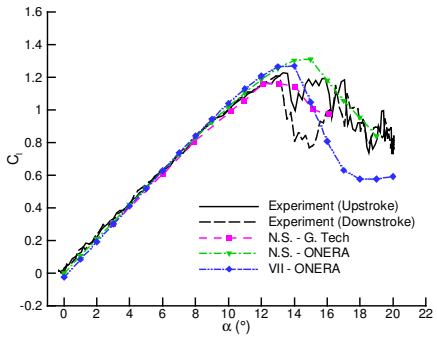


Figure 3 - Variation of lift with angle of attack

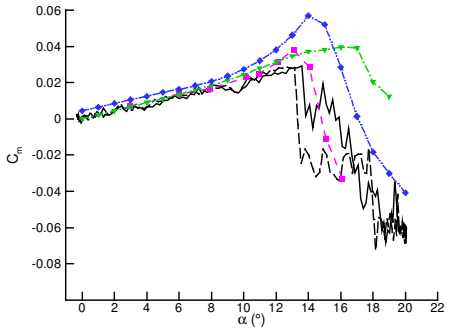


Figure 4 - Variation of pitching moment at the quarter-chord with angle of attack

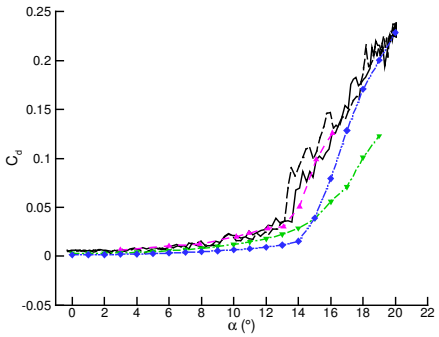


Figure 5 - Variation of drag with angle of attack

Oscillating Airfoil Calculations - Attached Flow

Following the steady flow studies, calculations were done for the airfoil oscillating at a reduced frequency *(k)* of 0.095. The angle of attack variation is given by:

$$\alpha = 4.0^{\circ} + 4.2^{\circ}\cos(\omega t)$$

At these low angles of attack, all the three methods gave quite comparable results. Figure 7 shows comparison of calculations from the analyses for the lift, pressure drag, and pitching moment data. The Georgia Tech N-S and ONERA N-S computations were carried out with an algebraic Baldwin-Lomax turbulence model in this particular case. From Fig. 7, it may be concluded that the present methods do a good job of predicting the variations in lift with angle of attack. The more sensitive pitching moments and drag

coefficients are less well predicted, but the overall trends for C_d and C_m are satisfactory.

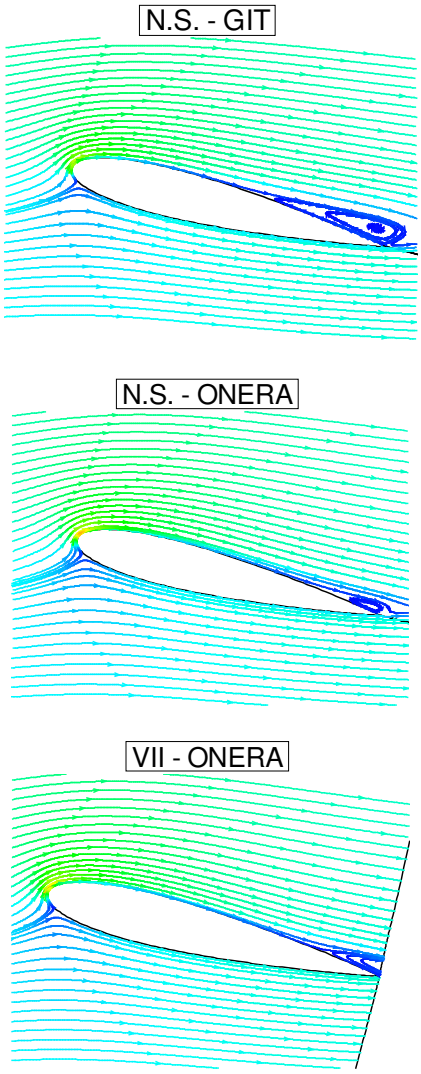


Figure 6. Computed static streamline patterns at 14 degree angle of attack

Moderate Stall Calculations – k = 0.095 and k = 0.038

Calculations have also been done for the airfoil oscillating at two reduced frequencies of 0.038 and 0.095 with the following angle of attack variation:

$$\alpha \cong 11.0^{\circ} + 4^{\circ}\cos(\omega t)$$

From the experimental data for these cases, it was found that the airfoil exhibits the moderate stall phenomenon at the low reduced frequency of 0.038, but experiences only a dynamic flow separation without full stall at the higher reduced frequency. These two cases have been selected specifically to determine whether the codes can capture accurately these differences observed in the experiments.

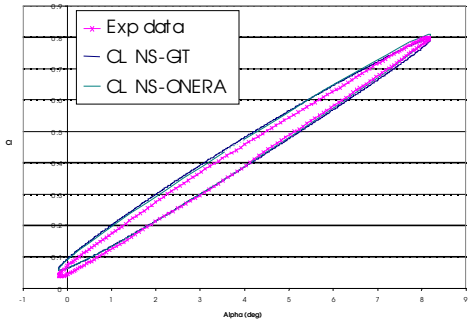


Figure 7*a. Variation of lift vs. α (attached flow, k=0.095)*

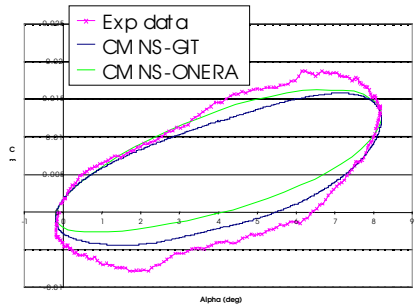


Figure 7*b. Pitching moment vs. α (attached flow, k=0.095)*

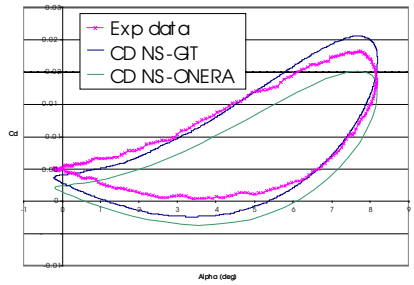


Figure 7c. Pressure drag vs. α (attached flow, k=0.095)

All subsequent computations with the Georgia Tech and ONERA NS codes are using a Spalart–Allmaras turbulence model, based on the knowledge that this turbulence model generally works better for the separated flow condition, when compared to Baldwin–Lomax model. The ONERA VII simulations were done using a two- equation model, with an automatic detection of transition.

Figures 8 and 9 show comparisons of lift, moment and drag hysteresis loops, for k = 0.095 and k = 0.038, respectively. The variation of the lift coefficient with angle of attack is well predicted by the two ONERA methods at k = 0.095, in particular for the VII method, that also performs better at k = 0.038. Georgia Tech method, as already seen in the static case, tends to underpredict the maximum lift and

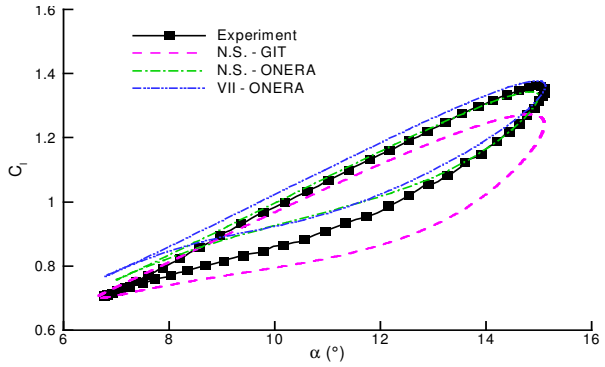


Figure 8a – Lift vs.α (moderate stall, k=0.095)

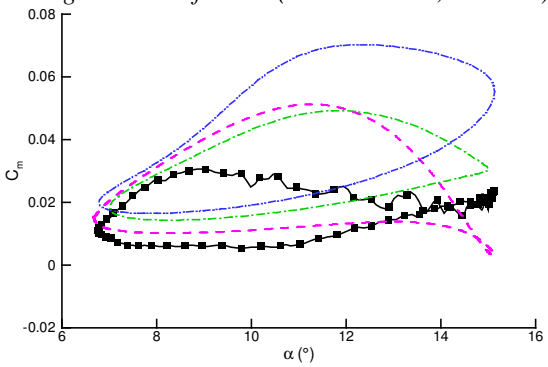


Figure 8b. Pitching moment vs.α (moderate stall, k=0.095)

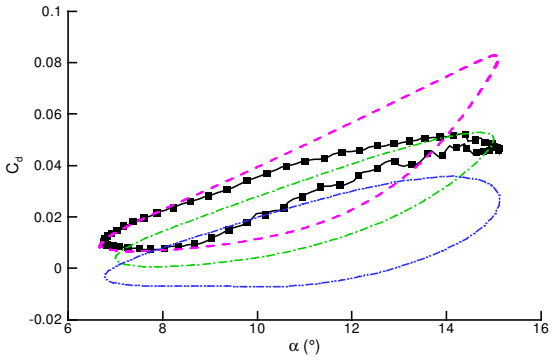


Figure 8c. Drag vs.α (moderate stall k=0.095)

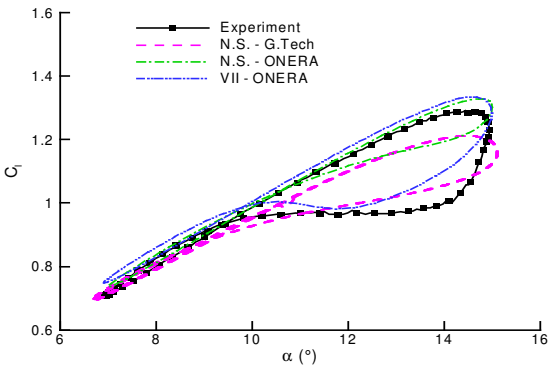


Figure 9a. Lift vs. α (moderate stall, k=0.038)

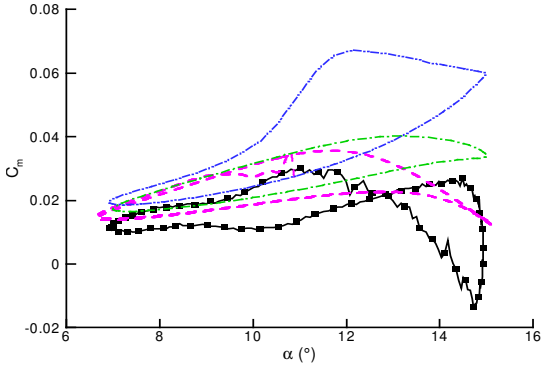


Figure 9b. Pitching moment vs.α (moderate stall, k=0.038)

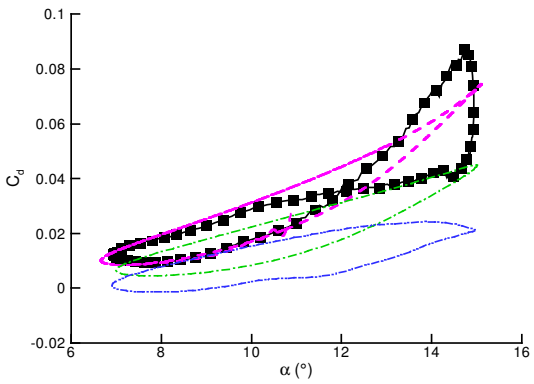


Figure 9c. Drag vs. α (moderate stall, k=0.038)

the slope of the curve in the linear part. None of the three methods could accurately predict either the occurrence of the nose-down pitching moment linked to the stall at the lower frequency of 0.038, or the drag evolution, at both frequencies.

To understand the inability of the methods to correctly predict the pitching moments and the mutual differences between these three methods, additional parameters such as the skin friction coefficient, flow reversal point, displacement thickness, pressure at a selected time and pressure in a complete cycle have been studied in detail. Since the pressure data are important for understanding the unsteady flow characteristics during the dynamic motion of the airfoil, discussion on the prediction of pressure data are presented here. First, the variations of Cp as a function of angle of attack are examined. Figures 10 and 11 show these results, at k = 0.095 and k = 0.038, respectively. Instantaneous surface pressure distribution at a typical angle of attack is shown in Fig. 12. It was observed that the leading edge suction peak is overpredicted by the ONERA methods relative to experiment during the upstroke resulting in a larger nose-up pitching moment, while the Georgia Tech methodology underpredicts the suction peak. During the downstroke, the Georgia Tech method produces a better agreement of pressures with experiments in the aft regions of

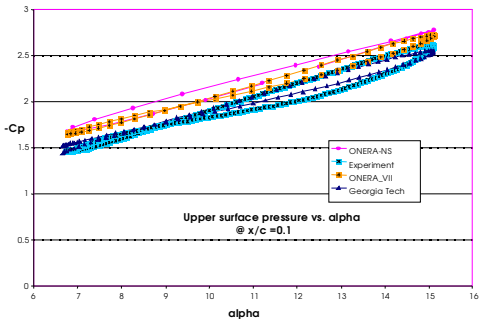


Figure 10a. Variation of Cp vs. angle of attack, moderate stall, k=0.095, x/c=0.1

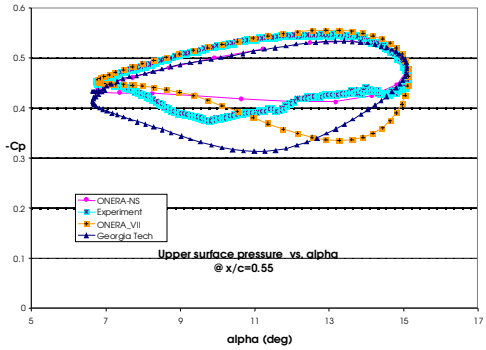


Figure 10b. Variation of Cp vs. angle of attack, moderate stall, k=0.095, x/c=0.55

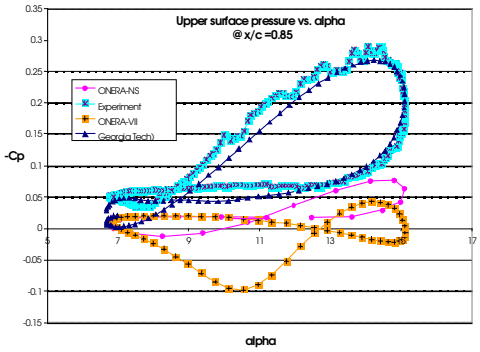


Figure 10c. Variation of Cp vs. angle of attack, moderate stall, k=0.095, x/c=0.85

the airfoil (Fig. 10c, 11b), in correlation with the underestimation of the pressure peak (Fig. 10a).

The reasons for these variations have been tracked to the following factors: a thicker boundary layer in the Georgia Tech analysis due to the inherent numerical viscosity in the method, the lack of a transition model in the Georgia Tech and ONERA-NS methods, and the sensitivity to transition and intermittency models in the ONERA-VII method. Further work is in progress to identify and reduce these sources of errors.

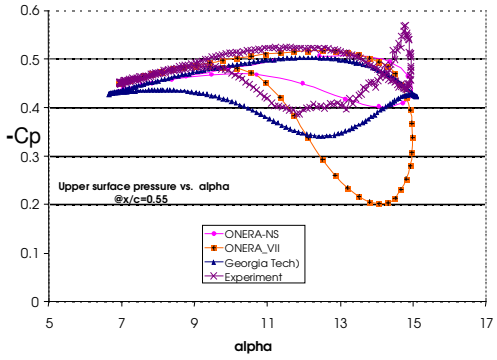


Figure 11a. Variation of Cp vs.angle of attack, moderate stall, k=0.038, x/c=0.55

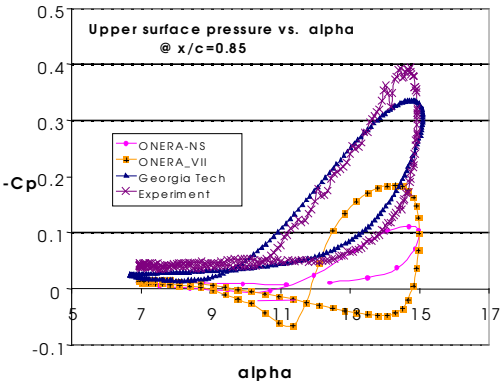


Figure 11b. Variation of Cp vs. angle of attack, moderate stall, k=0.038, x/c=0.85

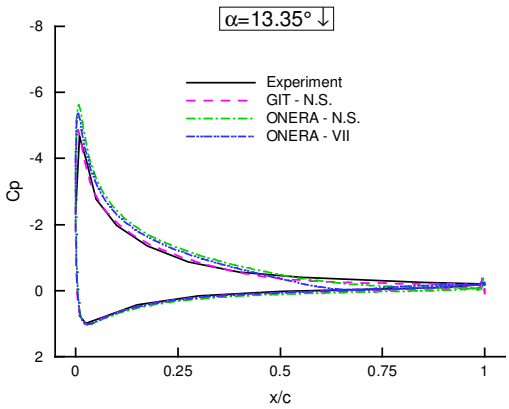


Figure 12. Moderate stall - k=0.038 – Instantaneous pressure coefficients - α=13.35° down stroke

Figures 13 and 14 show the instantaneous streamlines and Mach number contours for the three methods, at a particular angle of attack during the downstroke. It is seen that the Georgia Tech methodology (with the higher numerical viscosity coefficient of 0.2, compared to the value of 0.064 used in the ONERA-NS method) predicts a thicker boundary layer and a more pronounced and extended separation area, compared to the ONERA predictions. This thicker boundary

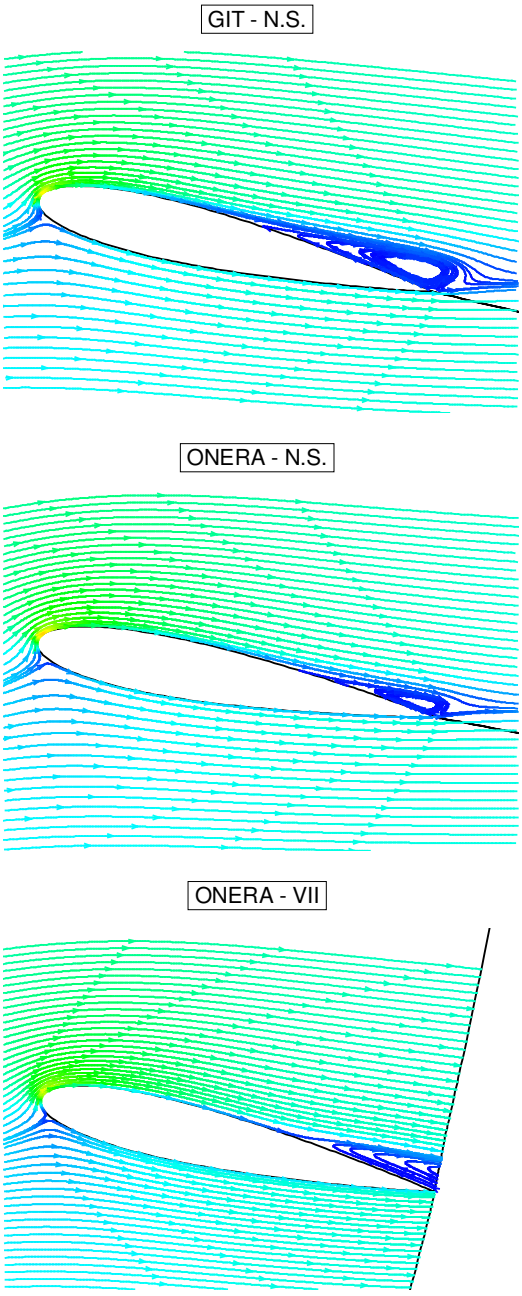


Figure 13. Moderate stall - k=0.038 – Streamlines around the airfoil - α=13.35° downstroke

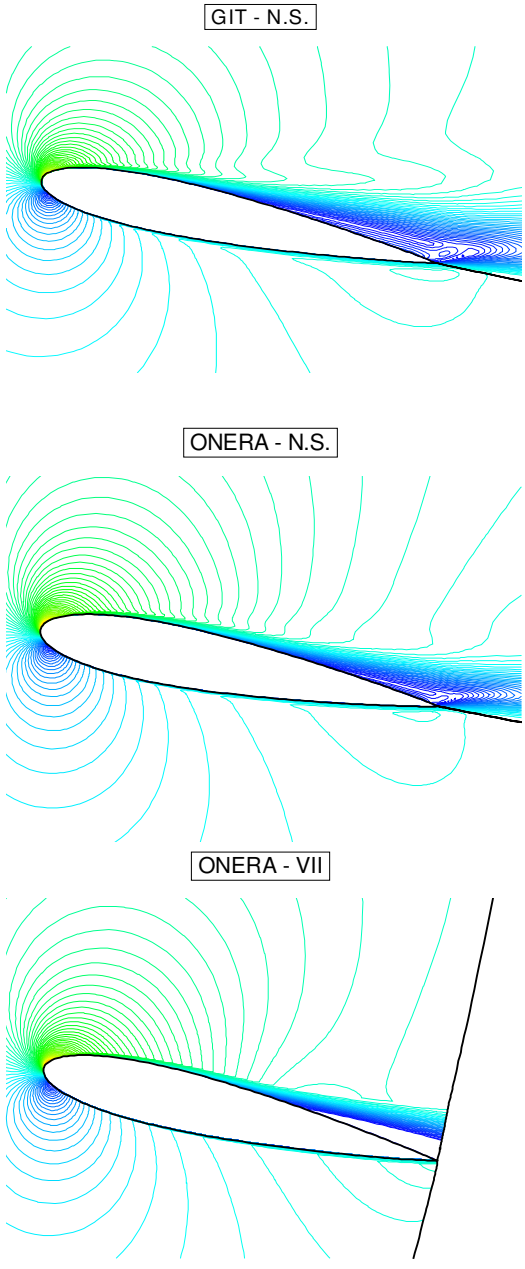


Figure 14. Moderate stall - k=0.038 – Mach number contours around the airfoil - α=13.35° downstroke

layer leads to a lower suction peak during the upstroke, and lower pressure values in the trailing edge region during the downstroke.

The qualitative shape of the iso-Mach contours also reveals differences between the three methods. It can be observed in thetwo RANS methods, with a different intensity in Georgia Tech and ONERA-NS results, the existence of a Mach number deficit, convected just above the viscous layer, that does not. appear in the ONERA-VII field, and that has been analyzed as an undue entropy layer.

Unsteadiness and Frequency Effects

As the reduced frequency is increased, experiments indicate a delay in the onset of stall, and an increase in the Clmax values. All the three methods predict qualitatively rather well the hysteresis at the higher reduced frequency,

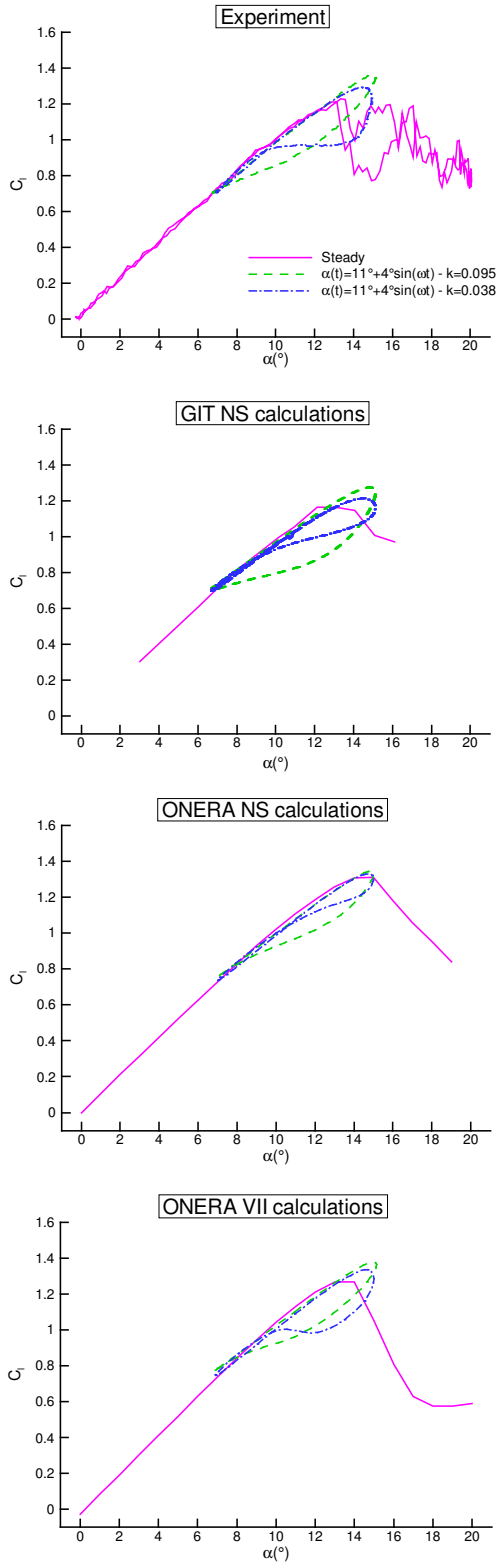


Figure 15. Moderate stall – restitution of unsteadiness and frequency effects.

in Figure 15. The stall delay and an extra unsteady lift over and above to the static lift is duly recovered by the Georgia Tech RANS method and the ONERA-VII method. The restitution of the frequency effect is somewhat better reproduced in its behavior and intensity by the ONERA-VII approach in this case.

Sensitivity Analysis to Grid Resolution for GIT Navier-Stokes Calculations

A limited set of calculations have been done to assess the effects of grid density on the calculations. A coarse 257x65 grid and a medium 257x129 grid were used.

Figure 16 shows the effects of grid on the computed lift and pitching moments in Georgia Tech method, while figures 17 and 18 show the streamline and Mach number contours at a typical instance in time.

As may be expected, the combination of a coarse grid and a high numerical viscosity was found to lead to an artificially thicker boundary layer on the 257x65 grid, and had profound effects on integrated loads. The agreement with experiment is surprisingly better with coarse grid than with finer grid.

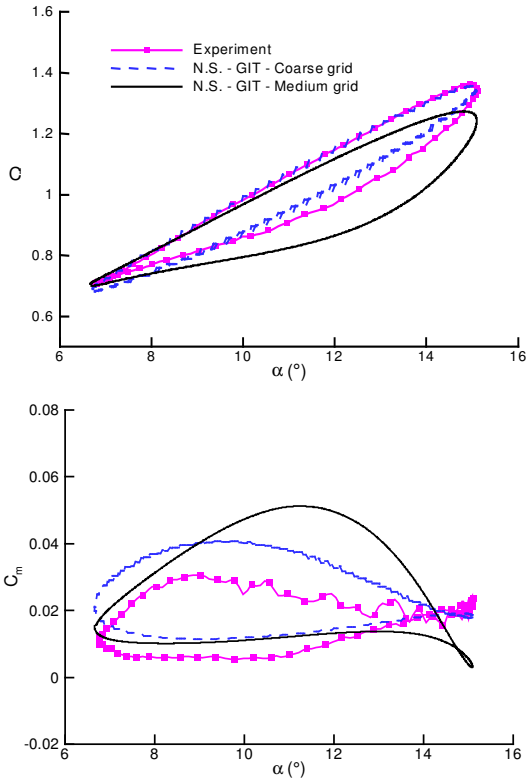
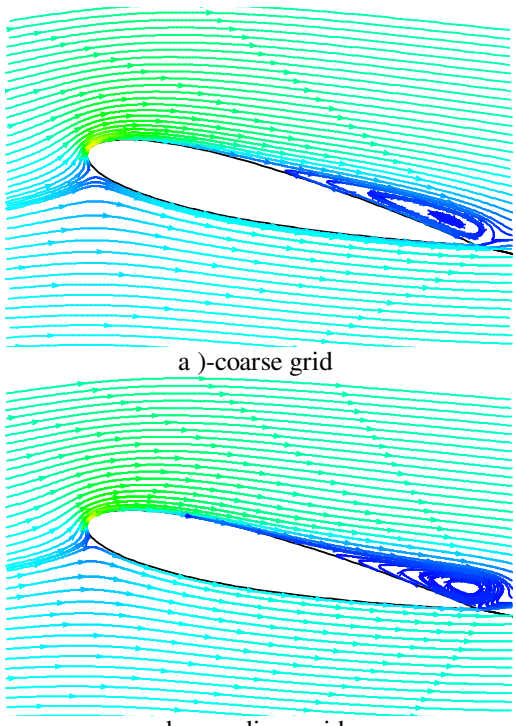


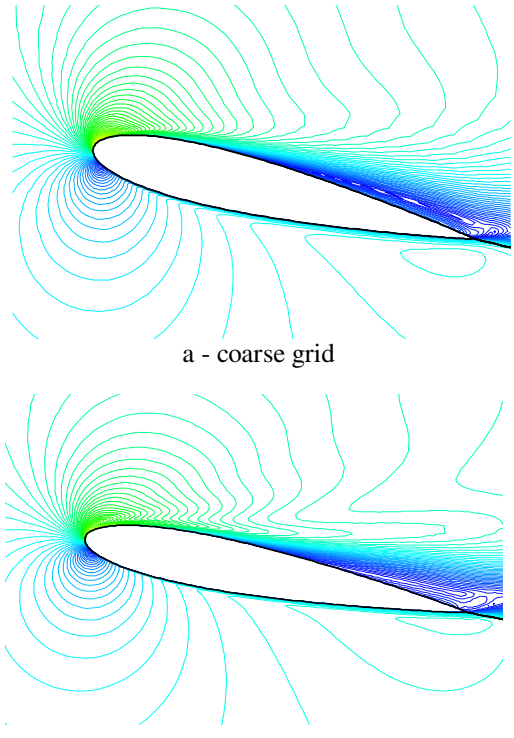
Figure 16. Influence of grid resolution on airload (Georgia Tech NS) .



a)-coarse grid

b – medium grid

Figure 17. Influence of grid resolution on streamlines around the airfoil (GIT-NS) - α=13.35° downstroke



a - coarse grid

B – medium grid

Figure 18.Influence of grid resolution in GIT-NS method, Mach number contours α =13.35° downstroke.

Effects of Numerical Viscosity on Hysteresis Loops in ONERA Navier-Stokes Calculations

The Jameson's dissipation coefficient can play an important role on the prediction of the separation phenomenon. To study these effects, a series of calculations were done with the ONERA-NS analysis, where the values of this coefficient χ4 generally vary from 0.016 to 0.064. Figure 19 clearly shows that the prediction of the lift hysteresis loop is modified when increasing the artificial viscosity coefficient χ4 from 0.032 to 0.064. In the linear part of the upstroke phase, as well as in the beginning of the downstroke phase, the Cl values are closer to the experiment. The width of the hysteresis loop is increased, and is closer to the experiment. Unfortunately, no real improvement of the evolution of the pitching moment coefficient is obtained. It has been verified that the decrease of the Cl value in the linear part, between 7° and 15°, for viscosity coefficient of 0.064 can be explained by the decrease in the pressure suction peak at the leading edge on the upper surface.

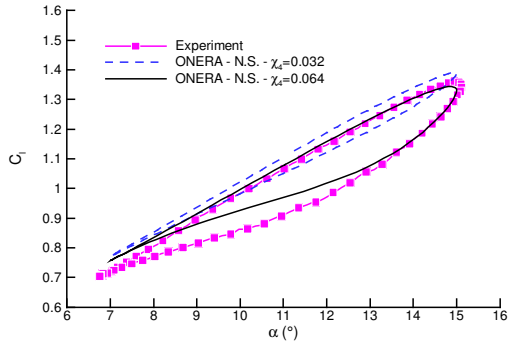


Figure 19. Influence of RANS artificial viscosity for ONERA Calculations – Comparison of lift coefficients.

Furthermore, near the trailing edge, for α=15° and α=13.35° downstroke (Figure 20), one can notice a larger extent of the flow separation from the trailing edge, when χ4=0.064. The influence of the χ4 coefficient on the velocity profiles, near the trailing edge (x/c=0.88), in the beginning of the downstroke phase (α=13.35°) is clearly shown in Figure 21. With χ4=0.032, the velocity field is always positive, and represents a slight beginning of flow separation. The thickness of the boundary layer is equal to 10% of the chord. With χ4=0.064, the velocity profile begins to be negative, which is linked to a flow reversal due to the separation phenomenon. Then, the velocity field becomes positive, and the thickness of the boundary layer (including the thickness of the separated flow) is equal to 14% of the chord. Finally, it has been checked that the increase of the artificial viscosity leads to, in some manner, a smaller level of eddy viscosity, especially for α=15° and

α=13.35° downstroke. This may explain the larger extent of the flow separation.

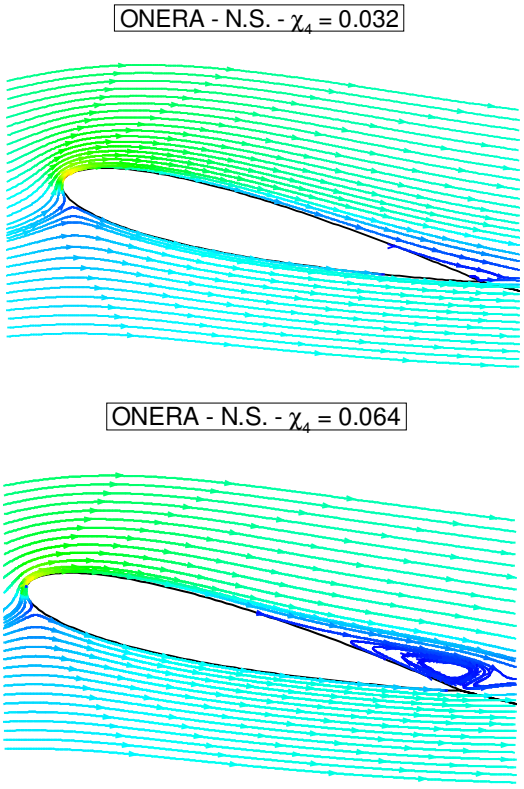


Figure 20. Influence of artificial viscosity on streamlines - α=13.35° downstroke

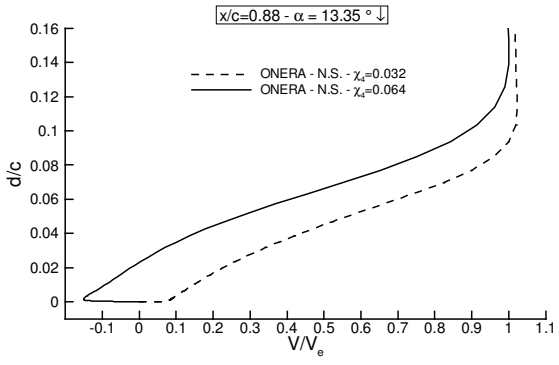


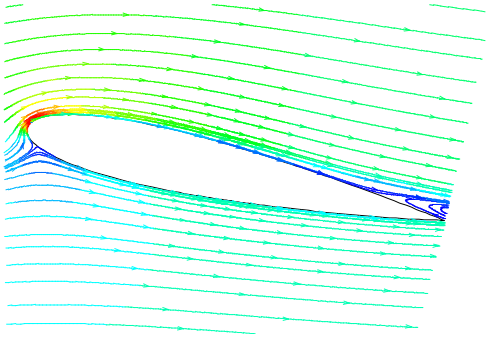
Figure 21. Influence of artificial viscosity - velocity profile in ONERA-RANS calculations

Sensitivity Analysis : Transition Influence from ONERA-VII calculation

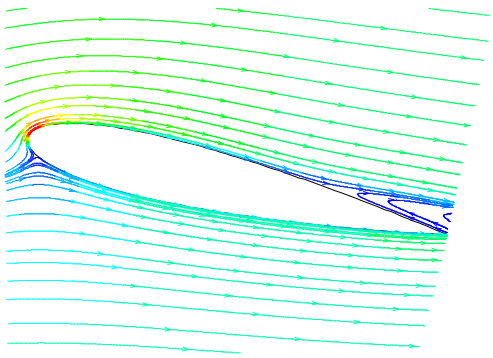
The viscous-inviscid approach VIS05 has indicated early in this study the importance of the transition treatment in such calculations at rather low Reynolds number. In all the cases reported here, static and dynamic ones, the VIS05 method predicts that the laminar separation occurs, on the upper surface, somewhat downstream the suction peak.

In the RANS codes that do not have an intermittency model and are run in a fully-turbulent mode, the intermittency of the transitional areas are unphysically simulated by the turbulence model, which in theory is not designed for this. Thus no conclusions can be drawn on the transitional flow restitution, the transitional bubbles and their bursting, and on the sensitivity of static or dynamic RANS computations to the beginning and to the extent of the transition.

The VIS05 code has an intermittency model, but the physical adequacy of this preliminary model is still acceptable only for attached flow, so that VIS05 computes the laminar or turbulent separated flows, but not yet the transitional ones. Then, the VIS05 method is reliable in the prediction of laminar separation, especially with its quasi-negligible numerical dissipation for predicting the thickness



a) Transition location prescribed at x/c=0.005



b) Transition location computed: Upstream, but very close to, instantaneous laminar separation

Figure 22 - Sensitivity to transition location given by VIS05 at moderate stall (k=0.095, α=13°, downstroke)

of the boundary layer along the laminar path. The method is also reliable in estimating the sensitivity of the flow computation to the location of the beginning of transition, when the transition is completed upstream laminar separation.

Figure 22 displays an example of the very high sensitivity of the flow that was found by VIS05, simply with minor changes in the beginning of a transition that is assumed to be fully completed upstream laminar separation. It is worthwhile to note that these small changes, implemented for example as a variation in the shape parameter of the laminar velocity profile for which the beginning of transition is assumed near separation, are found to have the same noticeable weight on the trailing-edge separation extent as the previously observed sensitivity of the RANS simulations to the grid refinement, and to the numerical diffusion.

It can be expected, then, that the sensitivity to intermittency models, and to transitional flow description, would be found larger and stiffer for simulations solving physically the transitional zones, that, in real flows, are spread within the separated flow regions themselves, both in the case of a leading-edge bubble, and in the case of a bursting of leading-edge separation.

CONCLUDING REMARKS - LESSONS LEARNED

Three different numerical methods have been applied to the static and dynamic stall characteristics of a NACA0015 airfoil. To avoid effects of different grid density, identical grids have been used for the two RANS methods. Despite the specificity of the VII method, the same streamwise grid as for RANS has also been maintained. These calculations aim at learning lessons for improving each method. Good agreement with experiments has been obtained for the static stall case, and for the attached flow. Large discrepancies between experiment and calculations were found for the moderate stall case.

At first glance, it is bewildering to see the variations in the predictions and the overall poor agreement with experiments for the moderate stall cases. A careful examination of the three methodologies indicates the following lessons.

1. All the results obtained with the ONERA generalized viscous-inviscid interaction method VIS05 show the presence of a laminar separation in all cases. The VIS05 solutions point out that the numerical capture of the physics (simply at RANS level, a fortiori in LES) requires streamwise grid refinement near laminar separation area and intermittency models for transitional flows description, in addition to the turbulence model.

2. The present VIS05 viscous-inviscid solutions, that are almost free of the undue numerical diffusion of RANS computations, and that benefit from a first step of intermittency model, have nevertheless assumed that transition is triggered by just upstream laminar separation. This unphysical temporary assumption probably delays the loss of leading-edge suction by laminar separation, and causes the residual deviations on drag and moment, at moderate stall, despite a rather favorable resolution of the static and dynamic lift.

3. Both in VII and RANS approaches, further progress is needed in the modeling of transition with intermittency models, and in the numerical capturing by the grid of laminar and transitional separations, in order to satisfy not only the normal discretisation inside the incoming boundary layer upstream separation, but also the discretisation of the streamwise length of the physical compression at separation.

4. Although the Georgia Tech and the ONERA Navier-Stokes methods have much in common in the way the governing equations and turbulent transport equation are discretized, there are notable differences in the way the Jameson-Turkel-Schmidt low past filter terms are treated. Both analyses require (as does the Jameson-Turkel-Scheme) the low pass filter to be scaled by a user specified coefficient. The lower values used in the ONERA method appear to produce a thinner boundary layer, less prone to separation, compared to the Georgia Tech method. It also leads in the ONERA simulations to an improved recovery of the pressure coefficient to its stagnation values near the trailing edge.

5. Further progress is needed in the discretisation of the numerical schemes for RANS methods. It will be advisable to perform further computations using minimal values of numerical viscosity to accurately study the effects of different physical modelings, such as turbulence and transition.

6. Beyond the only validation of the Balwin-Lomax and the Spalart-Allmaras turbulence models, it is worth investigating the use of two-equation turbulence model, for the moderate stall case, in conjunction with an appropriate transition model.

7. Further sensitivity studies of the RANS methods have also to be done, with higher grid density. Initial results on grid sensitivity indicate that the computations on the coarser grid provide a thicker boundary layer, and a more pronounced separation.

This study has been performed under a cooperative memorandum of agreement (MOA) in the area of helicopter aeromechanics between the US Army and the French SPAé at Ministry of Defense.

References

1. Ekaterinaris, John, A., and Platzer, Max F., "Computational Prediction of Airfoil Dynamic Stall," Progress in Aerospace Sciences, Vol. 33, pp. 759-846, 1997.

2. McAlister, K. W., Pucci, S. L., McCroskey, W. J., and Carr, L. W., "An Experimental Study of Dynamic Stall of Advanced Airfoil Sections, Vol. II- Pressure and Force Data," NASA TM-84245, September 1982.
3. Lorber, P. F. and Carta, F. O., "Airfoil Dynamic Stall at Constant Pitch rate and High Reynolds Number," Journal of Aircraft, Vol. 25, No. 6, pp. 548-556, June 1988.
4. Lorber, P. F., "Compressibility Effects on the Dynamic Stall of a Three-Dimensional Wing," AIAA Paper 92-0191, AIAA 30th Aerospace Sciences Meeting, January 1992.
5. H. Werlé, Possibilités d'essai offertes par les tunnels hydrodynamiques à visualisation de l'ONERA dans les domaines aéronautique et naval, Agard Conference Proceedings n° 413, October 1986, Mémoire n° 14.
6. Carr, L. W., and Chandrasekhara, M. S., "Compressibility Effects on Dynamic Stall," Progress in Aerospace Sciences, Vol. 32, pp 523-573, 1996.
7. Piziali, R. A., "2-D and 3-D Oscillating Wing Aerodynamics for a Range of Angles of Attack Including Stall," NASA TM 4632, September 1994.
8. Wu, Jiunn-Chi, Kaza, K and Sankar, L. N., "A Technique for the Prediction of Airfoil Flutter Characteristics in Separated Flow," Journal of Aircraft, Vol. 26, No. 2, February 1989, pp 168- 177.
9. A.M. Vuillot, V. Couaillier, N. Liamis, "3D Turbomachinery Euler and Navier-Stokes Calculations with a Multidomain Cell-Centered Approach". AIAA/SAE/ASME/ASEE 29th Joint Propulsion Conference on Exhibit, Monterey, CA, USA, 1993.
10. Collercandy, R., "Multigrid Strategy for Euler and Navier-Stokes Computations for Flows around Complex Aerospace Configurations," ECCOMAS CFD Conference, Athens, Greece, 1998.
11. Lerat, A., Sidès, J., Daru, V., "An Implicit Finite-Volume Method for Solving the Euler Equations," Lecture Notes in Physics, Vol. 17, Springer-Verlag Ed., 1982.
12. Liamis, N., Couaillier, V., "Unsteady Euler and Navier-Stokes Flow Simulation with an Implicit Runge-Kutta Method," ECCOMAS CFD Conference, Stuttgart, Germany, Wiley-Interscience-Europe Ed., 1994.
13. Rouzaud O., Plot S., Couaillier V., "Numerical Simulation of Buffeting over Airfoil using Dual Time-Stepping Method", ECCOMAS Conference, Barcelona, Spain, 2000.
14. Rouzaud O., Plot S., "Numerical Simulation of Unsteady Internal Flows using a Dual Time Stepping Method", 1st International Conference on CFD, Kyoto, Japan, 2000.
15. Rouzaud, O., Plop, A., "2D Unsteady Navier-Stokes Computations at ONERA for Prediction of Dynamic Stall," 24th European Rotorcraft Forum, Marseille, France, September 1998.
16. Le Balleur, J.C. - Strong matching method for computing transonic viscous flows including wakes and separations. Lifting airfoils. - La Recherche Aérospatiale 1981-3, p. 21-45, English and French editions, March 1981.
17. Le Balleur, J.C - New possibilities of Viscous-Inviscid numerical techniques for solving viscous flow equations, with Massive separation. – Proceedings Fourth Symp. Numerical and Physical Aspects of Aerodynamic Flows, Long-Beach,USA, January 1989, Selected papers, chap. 4, p. 71-96, editor T. Cebeci, Springer-Verlag 1990. (or ONERA.TP.1989-24).
18. Le Balleur, J.C. - Viscous-inviscid calculation of high-lift separated compressible flows over airfoils and wings. - Proceedings AGARD-CP-515, 1993, Paper 26, Banff, Canada, 5-8 october 1992, (or ONERA.TP.1992-184).
19. Le Balleur, J.C., Girodroux-Lavigne, P. - Calculation of Dynamic Stall by Viscous-Inviscid Interaction over Airfoils and Helicopter-blade Sections – Proceedings of the American Helicopter Society, 51st Annual Forum and Technology Display, Forth Worth, Texas, USA, May 9-11, 1995 (or ONERA TP 1995-37).
20. Le Balleur, J.C. - Viscous-inviscid flow matching : Numerical method and applications to two-dimensional transonic and supersonic flows. - La Recherche Aérospatiale 1978-2, p. 67-76 (March 1978). French, or English transl. ESA-TT-496.
21. Le Balleur, J.C. - Numerical viscous-inviscid interaction in steady and unsteady flows.-Proceed. 2nd Symp. "Numerical and Physical Aspects of AerodynamicFlows," Long-Beach, (1983), chap. 13, p. 259-284, T. Cebeci ed., Springer-Verlag 1984, (or ONERA.TP.1983-8).
22. Le Balleur, J.C. - Viscous-Inviscid interaction solvers and computation of highly separated flows. - "Studies of Vortex Dominated Flows,,chap. 3, p. 159-192, Proceed. ICASE symp. NASA Langley Field, USA, (July 9-10, 1985), Hussaini and Salas ed., Springer-Verlag 1987, (or ONERA.TP.1986-4).
23. A. Jameson, W. Schmidt, E. Turkel, "Numerical Solution of the Euler Equations by Finite Volume Methods Using Runge-Kutta Time Stepping Schemes," AIAA Paper 81-1259, 14th Fluid and Plasma Dynamics Conference, Palo Alto, CA, USA, 1981.
24. Jameson A., "Time Dependent Calculations using Multigrid, with Applications to Unsteady Flows past Airfoil and Wings, " AIAA Paper 91-1259, 1991.
25. Roe, P. L., "Approximate Riemann Solvers, Parameter Vectors, and Difference Schemes," Journal of Computational Physics, Vol.43, 1981 pp. 357-372.
26. Beam, R and Warming, R.F "An implicit finite difference algorithm for hyperbolic systems in conservation law form," Journal of Computational Physics, Vol 22. Sept 1976.
27. Spalart, P. R., and Allmaras, S. R., "A One-Equation Turbulence Model for Aerodynamic Flows," AIAA Paper 92-0439, 1992.